



1 **Boosting aerosol surface effects: Strongly Enhanced**
2 **Cooperative Surface Propensity of Atmospherically**
3 **Relevant Organic Molecular Ions in Aqueous Solution**

4 Harmanjot Kaur,¹ Stephan Thürmer,² Shirin Gholami,¹ Bruno Credidio,¹ Florian Trinter,^{1,3} Debora
5 Vasconcelos,⁴ Ricardo Marinho,^{5,6} Joel Pinheiro,⁷ Hendrik Bluhm,¹ Arnaldo Naves de Brito,⁷ Gunnar
6 Öhrwall,⁸ Bernd Winter,¹ and Olle Björneholm^{4*}

7
8 ¹*Fritz-Haber-Institut der Max-Planck-Gesellschaft, Faradayweg 4-6, 14195 Berlin, Germany*

9 ²*Department of Chemistry, Graduate School of Science, Kyoto University, Kitashirakawa-Oiwakecho,*
10 *Sakyo-Ku, 606-8502 Kyoto, Japan*

11 ³*Institut für Kernphysik, Goethe-Universität Frankfurt, Max-von-Laue-Straße 1, 60438 Frankfurt am*
12 *Main, Germany*

13 ⁴*Chemical and Biomolecular Physics, Department of Physics and Astronomy, Uppsala University,*
14 *75120 Uppsala, Sweden*

15 ⁵*Institute of Physics, Brasilia University (UnB), 70.919-970, Brasilia, Brazil*

16 ⁶*Institute of Physics, Federal University of Bahia, 40.170-115, Salvador, BA, Brazil*

17 ⁷*Department of Applied Physics, Gleb Wataghin Institute of Physics, Campinas University, CEP,*
18 *13083859, Campinas SP, Brazil*

19 ⁸*MAX IV Laboratory, Lund University, SE 22100 Lund, Sweden*

20

21

22

23

ORCID

24

ST: 0000-0002-8146-4573

25

SG: 0000-0002-0647-1490

26

BC: 0000-0003-0348-0778

27

FT: 0000-0002-0891-9180

28

RM: 0000-0001-5854-5589

29

HB: 0000-0001-9381-3155

30

ANdB: 0000-0002-9098-444X

31

GÖ: 0000-0002-5795-8047

32

BW: 0000-0002-5597-8888

33

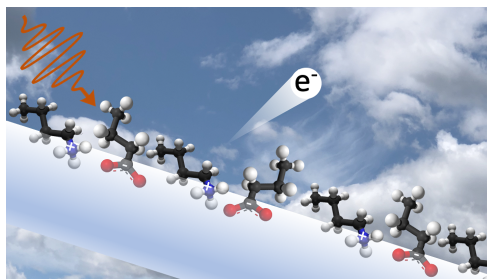
OB: 0000-0002-7307-5404



34

35

*Corresponding author: Olle Björneholm: olle.bjorneholm@physics.uu.se



36

37 **Abstract**

38 The effects of atmospheric aerosols are key uncertainties in climate models. One reason is the
39 complex aerosol composition which includes a relatively large fraction of organics. Another reason
40 is the small size of aerosols, which makes surface effects and processes important. These two factors
41 make surface-active organics important for atmospheric aerosols, as they can affect important
42 processes, such as chemical aging and water accommodation, as well as properties such as the surface
43 tension, which drives droplet formation. Two important types of atmospherically relevant organics are
44 carboxylic acids and alkyl amines, and often both are found together within aerosols. In the most
45 atmospherically relevant pH range, these exist as alkyl carboxylate ions and alkyl ammonium ions,
46 Using liquid-jet photoelectron spectroscopy, tuned to high surface sensitivity, we measured the alkyl
47 carboxylate cations and the alkyl ammonium anions of alkyl chain lengths 1 to 6 carbon atoms, both as
48 single-component and mixed-component aqueous solutions. This enabled us to systematically study
49 how their surface propensity is affected by the length of the alkyl chains, and how cooperative ion-ion
50 interactions result in strongly increased surface propensity. An exponential increase in surface
51 propensity is found for the single-species solutions, with cooperative solute-solute effects in mixed
52 solutions drastically increasing the number of molecules present at the solutions' surfaces up to a factor
53 of several hundred. This cooperative surface propensity is shown to strongly affect the amounts of
54 organics at the surface, with pronounced chain length-dependent variations. Our results demonstrate
55 that the surface composition of these water-organics systems can be very different from the bulk
56 composition, and that the surface compositions of organic mixtures cannot be directly inferred from the
57 behaviour of the single components. For aerosols containing these or similar species, this means that all
58 surface-related properties and processes will be enhanced, and the implication for atmospherically
59 relevant processes such as water accommodation, droplet formation, and chemical aging, is discussed.



60 Introduction

61 Water's liquid-vapor interface is of crucial environmental significance, considering the abundance
62 of liquid water covering Earth's surface, and of aqueous particles in Earth's atmosphere. The latter,
63 varying from microscopic aerosols to raindrops, impacts the global radiation balance by scattering
64 sunlight (the direct effect),(McCormick and Ludwig, 1967) and by serving as important cloud
65 condensation nuclei (CCN) and ice-nucleating particles (the indirect effects).(Twomey, 1974) The
66 effects of aerosols have been identified by the United Nations Intergovernmental Panel on Climate
67 Change (IPCC) as a key uncertainty in climate models,(The Intergovernmental Panel on Climate
68 Change (Ipcc), 2022) and thus a better understanding of these effects is important for improving climate
69 modeling. Atmospheric aerosols comprise many species, including atomic ions, organic compounds
70 from various sources like emissions and decomposition, soot from combustion, and mineral particles.
71 The organic fraction, ranging from 20-90% of submicron aerosol mass, mainly forms secondary organic
72 aerosols (SOA) with complex compositions.(Jimenez et al., 2009) The complex mix of organic
73 compounds within atmospheric aerosols makes it challenging to quantify the effect of aerosols on the
74 climate and associated climate changes.(Kanakidou et al., 2005; Tsigaridis et al., 2014)

75 The importance of aerosols stems from their large surface-to-volume ratio. One notable consequence
76 is that the surface concentration of atmospherically relevant amino acids is up to ten times higher than
77 inside the aerosols.(Mocellin et al., 2017) Furthermore, the surface concentration of amino acids tends
78 to increase upon addition of salt to the aqueous solution.(Gopakumar et al., 2022; Björneholm et al.,
79 2022) Yet, existing climate models often pay less attention to aerosol surface effects because
80 understanding of atmospheric surface phenomena on the molecular level is lacking.(Noziere, 2016;
81 Lowe et al., 2019) Specifically, aforementioned organics affect surface tension, altering condensation
82 and evaporation rates, which in turn alters water accommodation, *i.e.*, the aggregation of water mass
83 onto the aerosol.(Sareen et al., 2013; Ovadnevaite et al., 2017; Davies et al., 2013; Ergin and Takahama,
84 2016; Miles et al., 2016; Ruehl et al., 2016) As surface species are more accessible for reactions with
85 atmospheric radicals, the surface propensity of constituent species also affects the aerosol chemical
86 aging, *i.e.*, the time evolution of the chemical composition via chemical and photochemical
87 processes.(McFiggans et al., 2006; Shiraiwa et al., 2011) Microscopic surface effects are thus crucial
88 for aerosol growth and cloud condensation nuclei activity, thereby affecting the macroscopic radiative
89 forcing, *i.e.*, Earth's energy balance in terms of reflection and absorption of solar radiation.

90 A promising experimental approach towards a deeper understanding of the molecular-scale
91 interfacial structure and associated processes is the application of liquid-jet photoelectron spectroscopy
92 (LJ-PES) to selected molecular model systems in aqueous solutions in combination with X-rays tuned
93 to a surface-sensitive energy range. Many important organics are amphiphilic, *i.e.*, containing both
94 hydrophobic and hydrophilic parts; the former often consist of non-polar groups such as alkyl chains,
95 while the latter consist of polar or charged groups. The surface propensity of such amphiphiles can be



96 seen as a balance between the hydrophilic and hydrophobic interactions, where the hydrophilic part is
97 solvated while the hydrophobic part tends to be only partially solvated. For example, LJ-PES studies in
98 conjunction with molecular dynamics (MD) simulations have previously revealed how the surface
99 propensity increases and how the molecular surface orientation evolves with the length of the
100 hydrophobic alkyl chain for alcohols and carboxylic acids.(Werner et al., 2018; Ekholm et al., 2018;
101 Walz et al., 2016; Walz et al., 2015; Öhrwall et al., 2015; Lee et al., 2016) This picture has been
102 quantitatively corroborated for perfluorinated pentanoic acid in aqueous solution, for which the distance
103 of different parts of the molecule from the solution surface was determined with Angstrom resolution
104 from the analysis of photoelectron angular distributions.(Dupuy et al., 2023) The hydrophobic ends may
105 undergo orientational changes, from mainly aligned parallel (to the molecular axis with respect to the
106 surface plane) at low surface coverage towards perpendicular with increasing coverages to make room
107 for more molecules. Such reorientation was, for example, observed for alcohols in aqueous
108 solution.(Walz et al., 2015; Walz et al., 2016)

109 Two common types of hydrophilic functional groups in atmospherically relevant organics are
110 carboxyl/carboxylate and amine/ammonium (depending on pH, $-\text{COOH}/-\text{COO}^-$, and $-\text{NH}_2/\text{NH}_3^+$,
111 respectively), and carboxylic acids and alkyl amines are examples of amphiphiles commonly found in
112 aerosols.(Goldstein and Galbally, 2007) Both carboxylic acid and alkyl amines are considerably surface
113 active.(Werner et al., 2018; Ottosson et al., 2011) Most notably, in both cases larger alkyl-chain lengths
114 result in larger surface propensity. However, surface propensity is also pH dependent, with a smaller
115 surface propensity of the charged species as compared to the neutral ones. However, as discussed above,
116 atmospheric aerosols often contain multiple organic species. Interaction between different organic
117 solutes can affect their respective surface propensity, both via cooperative or competing effects.
118 Cooperative ion-pairing effects at the surface in mixed hexanoate/hexyl ammonium solutions were
119 shown to amplify the surface propensity of both species.(Ekholm et al., 2018)

120 It can thus be expected that the surface propensity of atmospherically relevant alkyl carboxylate ions
121 and alkyl ammonium ions scales with both the length of their hydrophobic chains and cooperative ion-
122 ion interactions. In this work, we systematically explore how both effects jointly affect a molecule's
123 surface propensity, exemplified for alkyl-carboxylate and alkylammonium ions of variable alkyl-chain
124 lengths. Our results provide insight into the molecular driving forces affecting the surface composition
125 of mixed-organic aqueous solutions, which will aid atmospheric scientists in creating a parameterized
126 description of aerosol surface phenomena for improving climate models.

127 **Methods**

128 **1. Experiments**

129 Most measurements of this study were performed using the *EASI (Electronic structure from Aqueous*
130 *Solutions and Interfaces)* liquid-jet photoelectron spectroscopy apparatus(Malerz et al., 2022) in tandem



131 with the P04 soft X-ray beamline(Viefhaus et al., 2013) of the PETRA III synchrotron radiation facility
132 (Deutsches Elektronen-Synchrotron DESY, Hamburg, Germany). Some measurements were repeated
133 at the PLÉIADES beamline of the SOLEIL synchrotron facility (Paris, France),PLÉIADES beamline
134 website, Synchrotron SOLEIL, Saint-Aubin, <https://www.synchrotron-soleil.fr/en/beamlines/pleiades>.
135 which is explained further below. The LJ-PES apparatus used at PETRA III is equipped with a state-
136 of-the-art, near-ambient-pressure hemispherical electron analyzer (HEA, Scienta Omicron HiPP-3),
137 complete μ -metal shielding, and large pumping capabilities for volatile liquids. Under operation
138 conditions, the average pressure in the interaction chamber was typically maintained at $\sim 2 \times 10^{-4}$ mbar,
139 as accomplished with two turbomolecular pumps (with a total pumping speed of ~ 2600 L s^{-1} for water)
140 and three liquid-nitrogen cold traps (with a total pumping speed of ~ 35000 L s^{-1} for water). A custom-
141 made differential pumping chamber, installed between the interaction chamber and the last beamline
142 element, ensures a sufficient pressure drop across three differential stages for connection to the
143 beamline.(Malerz et al., 2022) The circularly polarized light from the APPLE II undulator(Sasaki,
144 1994) of the P04 beamline was monochromatized by a variable-line-spacing monochromator using a
145 1200 l/mm planar grating (9 nm groove depth, non-blazed, Au coating) and a 150 μ m vertical exit-slit
146 opening (perpendicular to the LJ axis and the light propagation direction), adjusted by the exit slit unit
147 (EXSU). Photon energies of 400 eV (resolution of 70 meV) and 510 eV (resolution of 100 meV) were
148 employed to measure C 1s and N 1s photoelectron spectra, respectively. For a few solutes with very
149 high surface propensity, the C 1s PE signal could become so high to potentially saturate the detector.
150 This was prevented by reducing the photon flux by narrowing of the vertically oriented beam-defining
151 aperture (BDA), which is located 27.9 m downstream of the undulator and 43.1 m upstream of the
152 EXSU.(Bagschik et al., 2020) An overview of the used BDA settings, along with corresponding photon
153 flux values measured using a SXUV photodiode, can be found in the Supporting Information. The
154 beamline's vertical spot size (relevant for the LJ target) at the 150- μ m EXSU opening was ~ 50 μ m,
155 independent of the BDA gap, which is somewhat larger than the LJ diameter (see below). The horizontal
156 (along the liquid jet axis) spot size was ~ 180 μ m. The photoelectron detection axis was at an angle of
157 $\sim 130^\circ$ with respect to the light propagation axis, in the vertical plane, *i.e.*, the spectrometer is above and
158 tilted towards the beamline in the backward direction.(Malerz et al., 2022) The LJ axis is in the
159 horizontal (floor) plane and thus orthogonal to both the light propagation and electron detection axes.

160 Surface-sensitive PES measurements were performed with a photon energy resulting in a C 1s
161 photoelectron kinetic energy (KE) of ~ 100 eV, where the effective attenuation length (EAL), *i.e.*, the
162 probing depth into solution, is ~ 15 Å.(Thürmer et al., 2013) The samples were aqueous solutions of
163 alkyl carboxylate anions (sodium counter cation) and alkyl ammonium cations (bromine counter anion)
164 with variable chain lengths, with a total of 8 individual molecular species and 16 paired mixtures (see
165 Table 1). To keep descriptions concise, we adopt an abbreviated naming scheme, where letters A and
166 C refer to alkyl amines and alkyl carboxylates, respectively. In addition, we use numbers which
167 represent the number of carbon atoms, indicating the molecular chain length. For the former, the study



168 covers the methylammonium ($\text{H}_3\text{C-NH}_3^+$)_{aq} cation, which is thus labeled ‘A1’, A2 = ethylammonium
 169 ($\text{H}_3\text{C-CH}_2\text{-NH}_3^+$)_{aq}, A4 = butylammonium ($\text{H}_3\text{C-CH}_2\text{-CH}_2\text{-CH}_2\text{-NH}_3^+$)_{aq}, A6 = hexylammonium ($\text{H}_3\text{C-}$
 170 $\text{CH}_2\text{-CH}_2\text{-CH}_2\text{-CH}_2\text{-CH}_2\text{-NH}_3^+$)_{aq}, all with a Br^- anion. The latter covers C1 = formate (HCOO^-)_{aq}, C2
 171 = acetate ($\text{H}_3\text{C-COO}^-$)_{aq}, C4 = butyrate ($\text{H}_3\text{C-CH}_2\text{-CH}_2\text{-COO}^-$)_{aq}, and C6 = hexanoate ($\text{H}_3\text{C-CH}_2\text{-CH}_2\text{-}$
 172 $\text{CH}_2\text{-CH}_2\text{-COO}^-$)_{aq}, all with a Na^+ cation. Mixed solutions of equimolar concentration are denoted C_x /
 173 A_y, with x, y being the carbon count. An overview of all studied single-component solutions as well as
 174 paired mixtures with their abbreviated labels is given in Table 1; sketches of all molecules are presented
 175 in Figure 2C. The same table format is maintained throughout the manuscript when discussing
 176 quantitative peak intensities. Single-species solutions were prepared by dissolving methylammonium
 177 bromide (A1), of 98% purity, ethylammonium bromide (A2), of ≥98% purity, n-butylammonium
 178 bromide (A4), of ≥98% purity, n-hexylammonium bromide (A6), sodium formate (C1), of ≥99%
 179 purity, sodium acetate (C2), of ≥99% purity, sodium butyrate (C4), of 98% purity, or sodium hexanoate
 180 (C6), of 99-100% purity, each from Sigma-Aldrich, in demineralized water (conductivity ~0.2 μS/cm)
 181 to yield a 0.1 M concentration. At this concentration, the surface coverage of A6 is ~0.37 and of C6
 182 ~0.15 of the maximum coverage, *i.e.*, well below surface saturation.(Ekholm, 2018) Since A6 and C6
 183 have the highest surface propensities among the single species, all other species will exhibit a lower
 184 surface coverage. Mixture solutions were prepared by mixing equal volumes of the pure solutions,
 185 yielding solutions with the same total solute concentration, 0.1 M, and 0.05 M concentration for each
 186 species.

187 **Table 1:** Labeling scheme for the studied molecular species with varying chain lengths: carboxylic
 188 acids (C1-C6, vertical) and alkyl amines (A1-A6, horizontal). The eight single-component solutions
 189 (C_x and A_y, respectively) had a solute concentration of 0.1 M. The 16 mixed solutions (C_x / A_y, italic
 190 text) were prepared with 0.05 M of each constituent, yielding the same total concentration of 0.1 M.

alkyl amine

		name	-----	methylammonium	ethylammonium	butylammonium	hexylammonium
			label	A1	A2	A4	A6
carboxylic acid	formate	C1		<i>C1 / A1</i>	<i>C1 / A2</i>	<i>C1 / A4</i>	<i>C1 / A6</i>
	acetate	C2		<i>C2 / A1</i>	<i>C2 / A2</i>	<i>C2 / A4</i>	<i>C2 / A6</i>
	butyrate	C4		<i>C4 / A1</i>	<i>C4 / A2</i>	<i>C4 / A4</i>	<i>C4 / A6</i>
	hexanoate	C6		<i>C6 / A1</i>	<i>C6 / A2</i>	<i>C6 / A4</i>	<i>C6 / A6</i>

191

192 The aqueous solutions were injected into the vacuum chamber as a liquid jet via a silica-glass
 193 capillary nozzle with an inner diameter of 25 μm. The liquid was pumped via a Shimadzu LC-20 AD



194 high-performance liquid chromatography (HPLC) pump combined with an inline-degasser unit
195 (Shimadzu DGU-20A_{5R}), and then pushed through the glass capillary to yield a typical flow rate of
196 ~0.8 ml/min. The solution temperature was kept at ~10 °C by water-cooling the LJ rod using a chiller
197 unit; the temperature is expected to be a few degrees lower at the point of ionization (approximately 5
198 mm further downstream after the liquid is expelled into vacuum) of the liquid jet, due to evaporative
199 cooling. At larger distances from the injection point, the liquid jet breaks up into droplets due to
200 Rayleigh instabilities. (Winter and Faubel, 2006) The resulting liquid spray is collected (frozen out) at
201 the surface of a liquid-nitrogen cold trap, downstream of the flow direction. The distance between locus
202 of jet – light-beam interaction and the HEA was ~0.8 mm, and the entrance aperture of the latter also
203 0.8 mm diameter. Accurate positioning of the jet was achieved by a high-precision x-y-z manipulator
204 to which the LJ assembly is mounted. The optimal overlap of all axes was continuously monitored and
205 adjusted during the measurement to account for signal fluctuations from small jet position drifts.

206 Because of stability issues noticed during analysis of the C1/A1 mixture in the first campaign,
207 measurements of C1, A1, and their mixture (C1/A1) were repeated at PLÉIADES. Again, photon
208 energies of 400 eV and 510 eV were employed to measure C 1s and N 1s photoelectron spectra,
209 respectively. Here, the electron spectrometer was mounted such that the electron detection axis was
210 perpendicular to the plane of the electron orbit in the storage ring. The LJ axis lies in the horizontal
211 plane (plane of the electron orbit in the storage ring). The direction of propagation of the light, the
212 electron detection axis and the liquid jet were mutually orthogonal to each other. The angle between the
213 light-polarization vector of the linearly polarized light and the spectrometer axis was set to 55° which
214 is close to the magic angle. A Shimadzu LC-40 AD high-performance liquid chromatography (HPLC)
215 pump was used to pump the liquid, and push it through a glass capillary with 40 µm orifice diameter at
216 a flow rate of 2.7 ml/min. The LJ is then collected in liquid form by a heated copper-beryllium catcher.
217 Differential pumping is achieved by housing the complete LJ assembly in an enclosure within the
218 vacuum chamber while using small orifices for the insertion of the X-rays and the extraction of the
219 photoelectrons. The distance between the LJ and the entrance of the 300 µm stainless-steel skimmer of
220 the spectrometer was 1 mm. For more experimental details of the setup at PLÉIADES see Refs. (Malerz
221 et al., 2021; Powis et al., 2015).

222 2. Data Analysis

223 The analysis of measured electron counts as a function of electron KE was carried out using Igor Pro
224 (WaveMetrics, Sutter Instrument). First, the C 1s bands were fitted for all single-species solutions, *i.e.*,
225 the carboxylic acids (C1 to C6) and alkyl amines (A1 to A6) to extract peak shapes and widths.
226 Exemplary fits for the C2 and A2 aqueous solutions are presented in Figures 1, top and center panels,
227 respectively. The broad, featureless signal background, originating from inelastically scattered
228 photoelectrons, was approximated with a linear function, which is a simplification but the most stable
229 choice with only two fit parameters to vary. The signal contributions from the two carbon atoms, labeled



230 p1 and p2 in the figure, respectively, can be separated for both solutions; all C_x and A_y species feature
231 two distinct carbon signal contributions as we will detail later. A noticeable asymmetry of the C 1s
232 bands of the carboxylic acids arises from unresolved vibrational excitation. To keep the number of
233 fitting parameters preferably low, we chose asymmetric exponentially modified Gaussian
234 (EMG)(Grushka, 1972) functions to account for the vibration contributions. The alkyl amine C 1s bands
235 did not show any resolvable peak asymmetry and were best fitted with two (one in case of A1) Voigt
236 functions instead. A Voigt function yielded a better fit than a simple Gaussian function. The added
237 complexity of both the EMG and Voigt functions has no impact on the results for the mixed solutions:
238 the shape of the EMG (asymmetry parameter τ) and the Voigt function (Gaussian-to-Lorentzian width
239 ratio) were held fixed in subsequent fits to the spectra of the mixed solutions, which removed any
240 influence from these parameters. Indeed, for most of the solutions studied here, our procedure resulted
241 in good overall fits of the measured photoelectron spectra. There are few exceptions, where small
242 additional signals occur, which we attribute to contaminations of unknown origin. These features were
243 fitted with additional Gaussian functions (see the Supporting Information for details), but were not
244 included in the determination of intensities (measured as peak area) of the respective C 1s bands.

245 The mixed-solution spectra are fitted with a sum of the same number and type of functions as the
246 individual species, where the shape (asymmetry τ for the EMG and width ratio for the Voigt functions,
247 respectively) and peak width were kept fixed. Additional features from possible contaminants could not
248 be discerned (see below), and thus additional (Gaussian) functions were not included in the mixed-
249 solution fits. Since the contaminant features are small and not expected to be associated with a surface-
250 active species, their contributions to the PE spectra, if present at all, becomes diminishingly small as
251 peak intensities scale up rapidly for larger species. Figure 1(bottom) shows the C 1s fits for the C2/A2
252 mixed aqueous solution; the respective fits for the single-species solutions have been already introduced
253 in Figures 1 (top and center panels). The p2 bands are at similar positions for both the C_x and A_y species
254 and are thus strongly overlapping. In cases where both the C_x and A_y chains were present, *i.e.*, $x, y > 1$
255 for both species, the p1-p2 peak distance for A_y was set and held fixed to the result from the fit to the
256 single-component A_y spectra. We note that the separation into distinct peak contributions becomes
257 more difficult for species with increasing chain lengths. The spectral features of the chain carbons are
258 almost completely overlapping for all species, which is an inevitable fact of the (lack of) chemical shift.
259 In fact, for mixtures with the longest-chain alkyl amine A6, we had to additionally constrain the peak-
260 height ratio p1/p2 for the C_x component to reach a stable fit, because the signal contributions from the
261 chain for each constituent could not be discerned. This is a reasonable simplification since peak p1
262 of the C_x species is well separated in the spectrum and can serve as an anchor for the fit to determine the
263 height of peak p2 for a fixed p1/p2 ratio.

264 We note that some of our PE spectra were unintentionally recorded under conditions of detector
265 saturation (see the Experiments section) which disproportionally affects the signal intensity of the
266 strongest bands for these spectra. Measurements of some samples (with the highest intensity) were



267 repeated using a lower photon flux to circumvent saturation; the procedure is described in detail in the
268 SI. Another complication was discovered when analyzing the peak intensities for the sodium
269 formate/methylammonium bromide (C1/A1) solution: We found fluctuating PE signal intensities of up
270 to a factor of two during the initial measurement campaign. In that case, we have repeated the
271 measurements from the (nominally) same C1 and A1 as well as C1/A1 concentrations in a different
272 measurement campaign, using a different setup at the SOLEIL synchrotron radiation facility. Those
273 measurements used a different sample batch and showed no sign of contamination, which reassured us
274 that the sidebands in the initial data originated from contaminants. The signal intensities from the repeat
275 measurement were scaled by the C1 signal to match the initial data, and were used instead for the results
276 presented here.

277 C 1s (relative) peak intensities, $I(C_x)$ and $I(A_y)$, the main observables in this study, which reveal a
278 given species' variable and competing surface propensity, were quantified by normalization to the
279 smallest peak-intensity value, $I(C1)$, which is from aqueous-phase formate (C1). This normalization
280 factor is used throughout the work for the analysis of all peak-intensity values, and thus the results
281 represent a relative increase in surface propensity compared to formate. Peak intensities scale with the
282 number of ionization targets, the photoionization cross section, and the probing depth of the C 1s
283 photoelectrons. (Hüfner et al., 2005) Molecular photoionization cross-sections are unknown, but are
284 taken to be the same for all carbon atoms. In most cases, it is useful to present the data with the
285 dependence on the carbon number removed, by normalizing to the number of relevant carbon sites. For
286 example, when discussing the total peak intensity for C4, containing four carbons, the total intensity
287 value is divided by four, and in the case of the C2/A4 mixture, with a total of six carbon atoms, the total
288 intensity will be divided by six; such normalization will be stated in the caption.

289 In the case of the nitrogen-containing Ay species, we also recorded and analyzed the N 1s spectra.
290 This procedure is much simpler, as only a single peak is present for all species, and was fitted with a
291 single EMG function and a linear background. No contaminants were observed here, indicating that the
292 contaminants are not degraded alkyl amine molecules. N 1s peak-intensity values were arbitrarily
293 normalized to yield the same normalized intensity value as for the C 1s of methylammonium bromide
294 (A1) for better comparability. Furthermore, the peak-intensity values of the mixed species must be
295 adjusted for differences in molecular number density since each species in the mixed solutions had a
296 concentration of 0.05 M instead of 0.1 M for the single-species solutions. Thus, intensity values were
297 adjusted by a factor of two whenever relevant for a direct comparison.

298 We also analyzed the valence-band PE signal intensity based on a simple height comparison of the
299 water $1b_1$ (HOMO) band for each solution's spectrum with that of a representative (average) neat water
300 spectrum; see Figure SI-2 in the SI for details.



301 Results and Discussion

302 Figure 1 shows C 1s PE spectra for three samples, C2 (top panel), A2 (middle panel), and C2 / A2
303 (bottom panel). These spectra are representative of the spectra recorded for all samples listed in Table 1;
304 all PE spectra considered in the present study including the peak fits can be found in the SI as Figures
305 SI-4, SI-5 and SI-6. For both species, the spectra consist of two peaks: the peak p2 at the highest KE,
306 *i.e.*, lowest binding energy (BE), corresponds to the methyl carbon. The peak p1 at lower KE, *i.e.*, higher
307 BE, is due to ionization of the carboxylate carbon for C2, and ionization of the carbon atom next to the
308 ammonium group in the case of A2. The chemical shifts agree well with previous studies (Ekholm et
309 al., 2018; Ottosson et al., 2011) and can be qualitatively understood as follows. The higher BE (lower
310 KE) of the carbon next to N and O is due to the electronegative atoms N and O reducing the electron
311 density around the C atoms relative to the methyl carbon. The slight shift of the methyl-carbon peak
312 between C2 and A2 is due to the different charges of the C2 and A2 molecular ions. The spectrum of
313 the mixed C2/A2 solution can be understood as a sum of the C2 and A2 spectra, see the bottom panel
314 of Figure 1.

315 We briefly comment on the definition of ‘chain’ length for the C_x versus A_y species. The fact that
316 carbon is not part of the functional group for the A_y offsets, in practice as we see below, the chain length
317 of this species by one with respect to C_x. Thus, we can say that A2 has a chain length of two, whereas
318 C2 has only a chain length of one, as the carbon atom in the functional group is omitted. For this reason,
319 we introduce the *effective* chain length $k = x - 1 = y$ for the C_x and A_y species, respectively. Yet, for A_y
320 we can still distinguish between the carbon closest to nitrogen. The intensity of peak p1 will be treated
321 separately as needed, since it allows us to discuss molecular orientation.

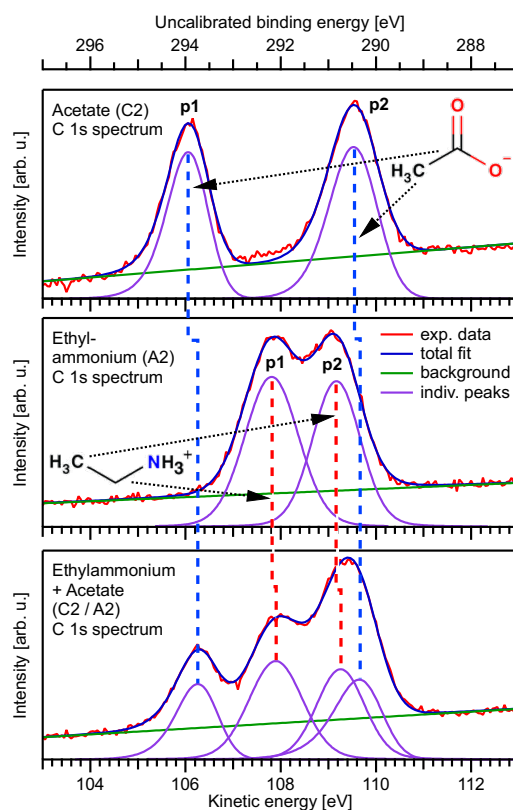
322 Single-component solutions

323 We start with the various single-component species in aqueous solution. Obtained peak intensities,
324 based on the analysis of the C 1s and N 1s PE spectra (see Methods), are summarized in Table 2 and
325 plotted in Figure 2A. Normalized total C 1s peak intensities, I_{norm} , for the carboxylate and alkyl
326 ammonium species are plotted on a logarithmic scale against the effective chain length k , which is a
327 measure of chain length ranging from 0 (no chain) to 6 (a six-carbon chain). Open circles represent
328 $I_{\text{norm}}(\text{C}_x)$ and $I_{\text{norm}}(\text{A}_y)$, respectively, crosses are I_{norm} of peak p1 only (related to the functional group),
329 and triangles represent I_{norm} for N 1s (A_y only). All values are normalized to the value of formate, $I(\text{C1})$,
330 and, as mentioned, the results can be understood as an increase in surface propensity relative to formate.
331 The values shown in the figure are further normalized to x , y , and thus any increase is solely due to an
332 increased surface propensity; see the bold numbers in Table 2 which are the ones plotted in Figure 2.

333 Formate is known to be repelled from the liquid–vapor interface, (Minofar et al., 2007) and thus can
334 serve as a baseline for quantifying surface activity for the series of molecules studied here. We can
335 attempt to isolate the surface contribution from the total intensity I_{norm} for a quantitative characterization



336 of the surface composition. Since all intensities have been normalized to the number of carbon atoms
337 (x,y), the normalized bulk contribution should be the same for all species, *i.e.*, equal to $I_{\text{norm}}(\text{C1})$. The
338 surface contribution is then obtained by subtracting $I_{\text{norm}}(\text{C1})$ from each value of the different solutions,
339 $I_{\text{surf, norm}} = I_{\text{norm}} - I_{\text{norm}}(\text{C1})$, which is equivalent to $I_{\text{surf, norm}} = I_{\text{norm}} - 1$ since all values are already
340 normalized by $I(\text{C1})$. This is done for both the Cx and the Ay species, and the resulting values are
341 plotted in Figure 2B. Clearly, the subtraction of the bulk component is just an approximation, since the
342 solution–vapor interface is not a sharp transition. In fact, there is an approximately 1-nm thick gradient
343 over which the molecular density changes; see, for example, Refs. (Werner et al., 2018) and (Minofar
344 et al., 2007) for the results of various organics. The $I_{\text{surf, norm}}$ values discussed from here on thus reflect
345 an average concentration within such a surface layer.



346
347 **Figure 1:** Exemplary C 1s PE spectra from aqueous solutions of 0.1 M sodium acetate (C2, top), 0.1 M
348 ethylammonium bromide (A2, center), and a mixture of sodium acetate and ethylammonium bromide
349 (C2/A2, both 0.05 M, bottom), plotted on the as-measured electron KE scale. The BE energy scale at the
350 top was calculated by subtracting the photon energy from the KE and was not further calibrated.
351 The two peaks p1 and p2 of the C2 spectrum, which are separated by a chemical shift, originate from



352 the methyl carbon and the carboxylate carbon, respectively. The two slightly overlapping peaks p1 and
 353 p2 in the A2 spectrum are from the methyl carbon and the carbon closest to the ammonium group,
 354 respectively. The spectrum of the mixed C2/A2 solution (bottom) can be understood as a sum of the C2
 355 and A2 spectra. For details of the fitting procedure, see Methods.

356 Except for the smallest molecules, C1 and A1, peak areas increase approximately exponentially with
 357 increasing k (note the logarithmic ordinate scale of Figure 2A), demonstrating a strong increase in
 358 surface propensity as the hydrophobic chain is extended. This is qualitatively expected given the well-
 359 known hydrophobicity of carbon chains. For $x = y$, the alkyl ammonium ions (A_y) have a somewhat
 360 higher surface propensity than the alkyl carboxylate ions (C_x), in agreement with the results for C4, C5,
 361 A4, and A6 in Ref. (Werner et al., 2018). Note again that the chain length for A_y includes the carbon
 362 next to the functional group, while for C_x the carbon inside the functional group is excluded to calculate
 363 the k values. A good match between C_x and A_y demonstrates that indeed the effective chain length and
 364 not the absolute number of carbons determines the surface propensity of these species.

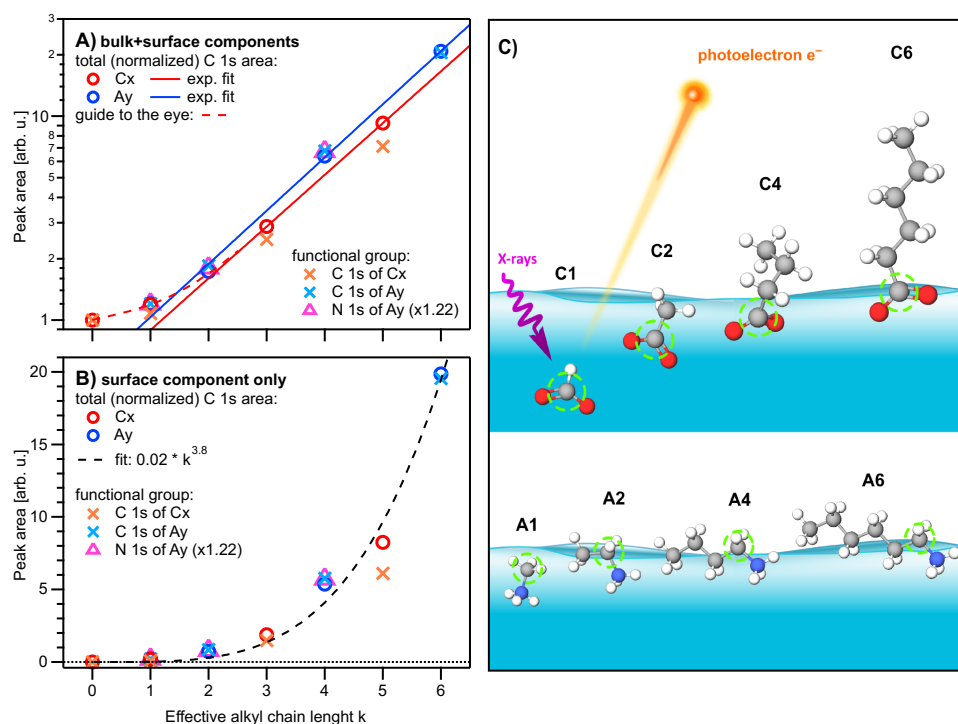
365 **Table 2:** Analysis results for each single carboxylic acid (C_x) and alkyl amine (A_y) solution extracted
 366 from peak fitting to the C 1s PE spectra. All peak intensities are normalized to the value of formate
 367 (C1); see Methods. Peak intensities increase approximately exponentially with increasing chain length
 368 for both the C_x and A_y species; compare Figure 2. The peak-intensity ratio R between peaks p1 and p2
 369 (see Figure 1) is compared to R_{ideal} , calculated from the number of carbons contributing to peak p2; only
 370 one carbon atom contributes to peak p1 for all species. The results reveal a deviation from unity for all
 371 species. $R / R_{ideal} > 1$ ($R / R_{ideal} < 1$) indicates a preferable orientation with the chain (the functional
 372 group) towards the surface. The bottom-most row reports the relative change in the valence-band signal
 373 of each solution compared to neat water; see also Figure SI-2. Bold values are plotted in Figure 2, panels
 374 A and B, respectively.

sample	C1	C2	C4	C6	A1	A2	A4	A6
effective chain length k	0	1	3	5	1	2	4	6
intensity I_1 of peak p1	1.00	1.08	2.49	6.75	1.20	1.85	6.76	20.55
intensity I_2 of peak p2	---	1.31	9.01	45.9	---	1.61	18.7	104.6
total: $I_{tot} = I_1 + I_2$	1.00	2.38	11.5	52.7	1.20	3.46	25.5	125.1
carbon-normalized $I_{norm} = I_{tot}/(x,y)$	1.00	1.19	2.87	9.25	1.20	1.73	6.37	20.86
total at surface: $I_{surf} = I_{tot} - I_{tot}(C1)$	0	1.38	10.5	51.7	0.20	2.46	24.5	124.1
normalize: $I_{surf,norm} = I_{norm} - I_{norm}(C1)$	0	0.19	1.87	8.25	0.20	0.73	5.37	19.86
peak-intensity ratio $R = I_2 / I_1$	---	1.21	3.63	6.80	---	0.87	2.77	5.09
ideal ratio $R_{ideal} (x-1 / y-1)$	---	1	3	5	---	1	3	5
ratio deviation R / R_{ideal}	---	<i>1.21</i>	<i>1.21</i>	<i>1.36</i>	---	<i>0.87</i>	<i>0.92</i>	<i>1.02</i>



relative valence-band signal	0.96	0.97	0.94	0.85	0.99	0.92	0.91	0.87
------------------------------	------	------	------	------	------	------	------	------

375



376

Figure 2: (A) Peak areas extracted from the fits to the PE spectra for each single-component solution of carboxylic acid and alkyl amine (Cx and Ay, respectively; x,y = 1,2,4,6), normalized by the value of formate, I(C1), and the number of carbons sites (x, y) within each molecule. Panel (B) shows the data of Panel (A) after additional subtraction of I(C1) which represent the surface contributions (see text); note the different vertical axis scales. All values are plotted against the effective chain length k (bottom axis). Red and blue open circles represent the total-area values $I_{tot} = I_1 + I_2$, i.e., a sum of all C 1s intensities, of the Cx and Ay species, respectively. Orange and light-blue crosses represent C 1s intensities of only peak p1 (related to the functional group) for Cx and Ay, respectively (compare Fig. 1). The N 1s peak intensities of Ay are plotted as purple triangles, which coincide with the crosses for Ay (i.e., the carbon near the functional group) when scaled with an arbitrary factor of 1.22. Both Cx and Ay show an approximately exponential increase as a function of k; note the logarithmic scale in panel (A) and the red and blue lines, which are exponential fits to the Cx and Ay data, respectively. Both species deviate somewhat from the exponential trend at low k, indicating a weaker promotion of surface propensity by short chains; see the red dashed curve as a guide to the eye. Small deviations of the crosses (functional group) above (Ay) or below (Cx) the circles (total intensity) values are due to molecular orientation (see text). (C) Sketch of the likely average depth and orientation of each species



393 as inferred from the absolute and relative intensities. The carbon site producing peak p1 is marked with
394 a green circle.

395 The surface contributions (Figure 2B) for both species exhibit similar behavior and can be
396 approximately described by $I_{\text{surf, norm}} \approx 0.02 k^{3.8}$. This is an arbitrary function obtained by fitting the data
397 without any theoretical justification. Yet, we would like to showcase the possibility of a parametrized
398 description of surface propensities, which would foster an inclusion of surface phenomena in improved
399 atmospheric models. We have also analyzed corresponding intensity changes of the solvent, *i.e.*, the
400 reduction of (water) valence-band PE signal intensity as a function of x,y compared to an average neat-
401 water valence spectrum. Results are shown in Figure SI-2B.

402 From the relative intensities between peaks p1 and p2, *i.e.*, the intensity originating from the carbon
403 close to or within the functional group I_1 relative to that from the chain carbons I_2 , we can also obtain
404 information about the average molecular orientation at the surface. Returning to Figure 2A, we take a
405 closer look at the peak intensities, I_1 (crosses), in close relation to the functional group; this carbon site
406 can be easily identified in the C 1s PE spectra due to its associated large chemical shift. A similar but
407 not exactly matching trend to the normalized total peak intensity, I_{norm} , is observed. For Ay, I_1 values
408 tend to be slightly higher than I_{norm} (compare circles vs. crosses); this is mirrored in the behavior of the
409 N 1s data (triangles). For Cx, the I_1 values tend to be somewhat lower than I_{norm} . Both effects can be
410 interpreted to originate from molecular orientation: if one end of the molecule is closer to the solution-
411 vapor interface, its signal will be larger compared to other molecular sites, which are pointing further
412 into the bulk solution. We quantify this by calculating the intensity ratio R between the peaks, *i.e.*, $R =$
413 I_2 / I_1 . This ratio can then be compared to R_{ideal} , calculated from the number of carbons contributing
414 only to peak p2, *i.e.*, the chain. If $R = R_{\text{ideal}}$ then all carbon sites are exposed equally (they are at equal
415 probing depths) on average, implying that the molecules are either parallel to the surface along their
416 long axis or randomly oriented. If instead $R / R_{\text{ideal}} \neq 1$, the molecule is preferably oriented normal to
417 the interface (anchored) with one end. Table 2 (bottom part) summarizes the values of R, R_{ideal} , and $R /$
418 R_{ideal} for each species. It is apparent that the ratio R / R_{ideal} is consistently above unity for Cx, which
419 implies that the Cx molecules are oriented with the hydrophilic functional group towards the bulk
420 solution, and the hydrophobic chain towards the vacuum. For Ay, the opposite trend is observed: $R /$
421 R_{ideal} is slightly smaller than unity. This is surprising since it implies that the (carbon near the) functional
422 group is closer to the interface than the chain. That is, the molecule lies rather parallel in the interfacial
423 plane, despite the hydrophilic interaction of the amine end. The proposed orientations and relative
424 depths of both species are sketched in Figure 2C.

425 To summarize, the single-component aqueous solutions of carboxylate anions and alkyl ammonium
426 cations show an approximately exponentially increased surface propensity as a function of length of the
427 hydrophobic alkyl chain. For the *same number* of carbon sites (*i.e.*, $x = y$), the surface propensity is
428 higher for alkyl ammonium cations than for carboxylate anions, consistent with the larger *effective* alkyl



429 chain length k of the former ($k = x - 1 = y$) and previous results for C4, C5, A4, and A6 in Ref. (Werner
430 et al., 2018). Moreover, the carboxylate anions seem to have an orientation perpendicular to the surface
431 plane, whereas the alkyl ammonium cations lie parallel to the surface plane

432 **Mixed solutions**

433 We now turn to the mixed solutions, with results summarized in Table 3 and plotted in Figure 3.
434 Analogous to Figure 2, Figure 3 shows the total normalized intensity I_{norm} in panel (A) and the surface
435 contribution $I_{\text{surf,norm}}$ in panel (B), with the latter also summarized in the table. To emphasize the changes
436 in surface composition, the normalized total surface intensity, $I_{\text{surf,norm}}$, a measure of the combined
437 amount of organic molecular ions at the surface, is derived as before for the single-component solutions
438 as $I_{\text{surf,norm}} = I_{\text{norm}} - I_{\text{norm}}(\text{C1})$. In the figure, results for the Cx and Ay single-species solutions are
439 highlighted by the red and blue circles, respectively. Values vastly increase for the mixed solutions,
440 Cx/Ay. Comparing $I_{\text{surf,norm}}$ for the two mixtures of the smallest, C1/A1, and largest molecules in this
441 study, C6/A6, we find an increase by a factor of ~ 230 . Neglecting depth-distribution differences, one
442 can directly relate this to the different number of molecular ions at the surface.

443 To quantify cooperative effects, we can make the ansatz that in absence of such effects the intensity
444 should just be the sum of the individual species' intensity, $I_{\text{sum}} = I(\text{Cx}) + I(\text{Ay})$. We then compare this
445 with the measured intensities for each mixture by calculating the ratio $R_{\text{coop}} = I_{\text{surf,norm}} / I_{\text{sum}}$; the resulting
446 values are summarized in Table 4. A ratio larger than unity corresponds to a larger than expected surface
447 propensity. This is more and more the case towards longer chain lengths, *i.e.*, higher x, y values. The
448 increase in the mixed solutions clearly shows that ion–ion interactions lead to a cooperative surface
449 enrichment of the organic molecular ions. We can discern roughly two regimes analogous to the single-
450 species results: a slow increase and small cooperative effect when the chain is short (absent) and a large
451 effect for long chains. For mixtures with C1 and C2 only an insignificant cooperative effect is observed;
452 C2/A1 is an exception, but we assume this is an outlier produced by a too high relative signal intensity
453 for this mixture in the experiment. For larger x, y the increase is more pronounced, reaching up to a
454 factor of three for C6/A4. We would expect the ratio for the C6/A6 mixture to be higher, but it is
455 possible that the surface already becomes saturated with molecules in this mixture, leading to a
456 relatively small increase as compared to the (already very surface-active) individual species C6 and A6.
457 We would like to emphasize at this point that surface saturation is another crucial aspect determining
458 the availability of molecular ions at the surface; here, saturation plays a limiting role for enrichment.
459 We have seen above that cooperative effects can multiply the number of molecules at the surface by a
460 factor of several hundred, which can quickly saturate the surface even at small bulk-solution
461 concentrations. Thus, the relative increase in number density may be much larger at small initial
462 concentrations very far from saturation, while only a small or even no enrichment may be observed for
463 an already relatively high initial concentration of each constituent species. Surface saturation should
464 thus always be considered when modeling ion densities. We also note that an asymmetric mixture

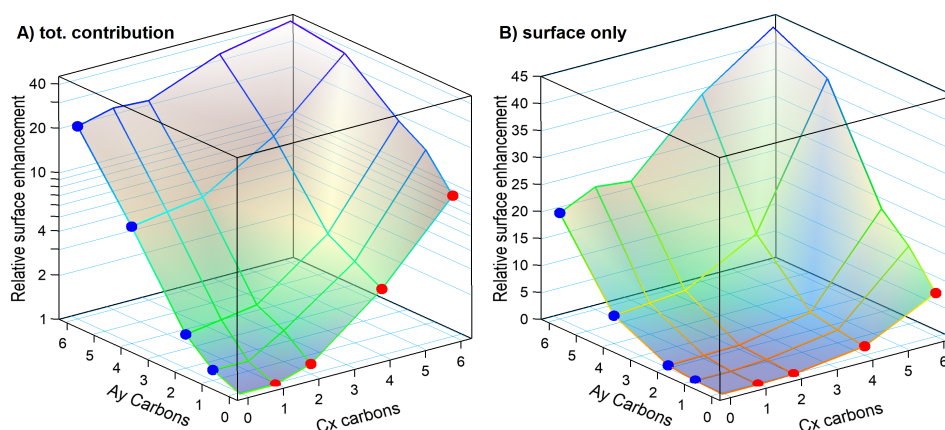


465 (deviations from the 1:1 concentration ratio) may further complicate the interaction, which is, however,
 466 beyond the current study.

467 **Table 3:** Total surface intensity, $I_{\text{surf, norm}}$, of all C 1s peaks and species combined, *i.e.*, the sum of all
 468 C 1s peaks not separated into different molecular sites, which were extracted from fits to PE spectra of
 469 single- (frame) and mixed-species (italic text) solutions; the former values are included for comparison
 470 and are the same as in Table 2. All peak intensities were normalized to the value of formate (C1) and
 471 to the relevant number of carbons (see Methods). Furthermore, values have been adjusted for
 472 differences in molecular number density, *i.e.*, 0.05 M (mixtures) *versus* 0.1 M (single species). The
 473 error for all values is estimated to be ± 0.05 from intensity fluctuations and fit errors.

		A1	A2	A4	A6
single	----	0.20	0.73	5.37	19.86
	mix:				
C1	0.00	<i>0.19</i>	<i>0.88</i>	<i>5.94</i>	<i>22.92</i>
C2	0.19	<i>0.73</i>	<i>1.05</i>	<i>6.53</i>	<i>22.24</i>
C4	1.87	<i>2.65</i>	<i>3.64</i>	<i>13.58</i>	<i>34.91</i>
C6	8.25	<i>14.66</i>	<i>19.31</i>	<i>38.93</i>	<i>43.85</i>

474



475

476 **Figure 3:** (A) Normalized total C 1s peak intensity, I_{norm} , *i.e.*, divided by the total number of carbon
 477 atoms and by the value of C1, for all studied species on a log scale. (B) Total surface component only,
 478 $I_{\text{surf, norm}}$, *i.e.*, after subtraction of $I(\text{C1})$, on a linear scale. The two abscissae represent the total number
 479 of carbons (x,y) in the molecule for Cx and Ay, respectively. Red and blue circles mark the values for
 480 each single-species solution Cx and Ay, respectively, and correspond to the red and blue circles in



481 Figures 2. The plots can be seen as analogous to Figures 2A and 2B but now including the mixed
482 solutions as a pseudo-3D representation. The highest overall surface propensity is observed for C6/A6.

483 **Table 4:** Surface enhancement ratio $R_{\text{coop}} = I_{\text{surf, norm}} / I_{\text{sum}}$ for the mixed solutions relative to the sum of
484 the individual species' intensity $I_{\text{sum}}(\text{Cx}/\text{Ay}) = I_{\text{surf, norm}}(\text{Cx}) + I_{\text{surf, norm}}(\text{Ay})$, using $I_{\text{surf, norm}}$ from Table 3.

	A1	A2	A4	A6
C1	0.95 ± 0.29	1.21 ± 0.12	1.11 ± 0.05	1.15 ± 0.05
C2	1.69 ± 0.23	1.14 ± 0.10	1.17 ± 0.05	1.11 ± 0.05
C4	1.28 ± 0.07	1.40 ± 0.06	1.88 ± 0.05	1.61 ± 0.05
C6	1.84 ± 0.05	2.27 ± 0.06	2.96 ± 0.06	1.59 ± 0.05

485

486 **Microscopic mechanism for cooperative surface enrichment**

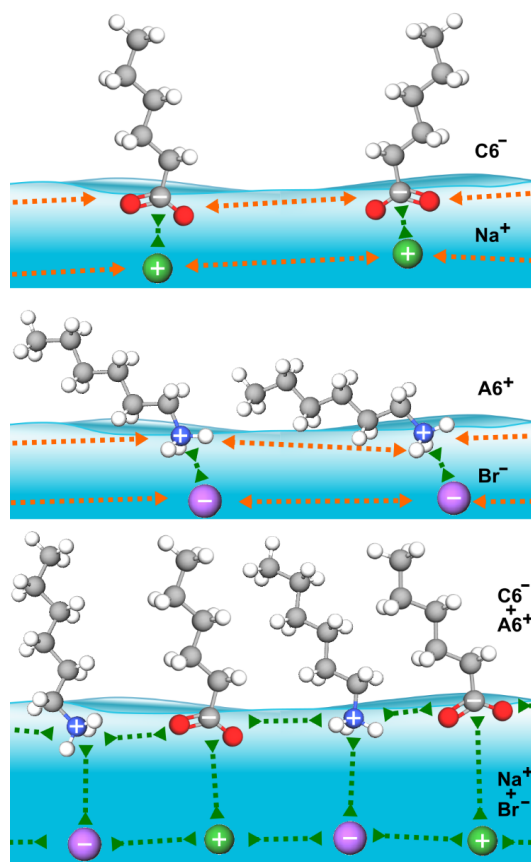
487 When only a single molecular ion species is present, the molecular ions on the surface repel each
488 other via their charged headgroups while their inorganic counter ions are located beneath the surface
489 layer, as schematically illustrated in Figure 4. Coulomb repulsion makes a high surface coverage of
490 molecular ions energetically unfavorable. However, in the mixed-solute systems, Coulomb repulsion is
491 reduced as the alkyl-ammonium cations and alkyl-carboxylate anions act as counter ions for each other,
492 fostering a cooperative effect that allows for greater coverage of organic molecular ions at the surface.
493 Cooperative surface enrichment similar to the observation in the present study has been reported for the
494 C6/A6 system, (Ekholm et al., 2018) and was qualitatively attributed to a combination of ion-pairing
495 between the charged functional groups of the respective organic ion, hydrophobic expulsion of the alkyl
496 chains from the surface, and van der Waals interactions between the alkyl chains. Furthermore, the close
497 packing of the alkyl chains contributes to the effect: Molecules align perpendicular to the surface and
498 are stabilized by van der Waals interactions between the chains, analogous to alcohols. (Walz et al.,
499 2015; Walz et al., 2016)

500 **Surface orientation**

501 For the single-species solutions, we concluded from the C 1s peak-intensity ratios, $R = I_2/I_1$, between
502 intensities originating from the carbon close to or within the functional group I_1 relative to that from the
503 chain carbons I_2 , that the Cx anions seem to have an average orientation perpendicular to the surface
504 plane, whereas the Ay cations are rather lying parallel to the surface plane. What then is the molecular
505 orientation in the mixed cases, considering the much higher molecule number densities at the surface?
506 In Table 5, we present the C 1s peak-intensity ratios R and R / R_{ideal} as defined for the single-component
507 cases. Again, a value of R / R_{ideal} above (below) 1 indicates a preferable orientation with the chain (the
508 functional group) closer towards the surface. We observe that the Cx species retain their preferential



509 perpendicular orientation, as expected. Similarly, the Ay species largely maintain their preferentially
510 parallel orientation for the most part. Interestingly, the data shows Ay changing into a perpendicular
511 orientation for C6/A4, C6/A6, and C4/A6, which hints at a configuration that is normal to the surface
512 and thus aligned with Cx at the surface. Note however, that the results for the latter two cases are less
513 reliable, since the peak ratio I_2/I_1 was constrained for the Cx component, thus possibly arbitrarily
514 inflating the ratio for Ay. Still, such a result may not be unexpected considering that a close packing of
515 aligned molecules would use the available space more effectively (compare Figure 4, bottom panel).
516 This result may also be related to the particular concentration likely reaching surface saturation, which
517 has the tendency to force molecules into an aligned configuration.



518
519 **Figure 4:** Schematic illustration of attractive (green arrows) and repulsive (orange arrows) interactions
520 between the organic and inorganic ions in the surface region for the C6 (top), A6 (middle), and C6/A6
521 (bottom) cases.



522 **Table 5:** Relative C₁s peak-intensity contribution from the chain I₂ versus the functional group I₁ for
 523 (A) the C_x and (B) the A_y species in aqueous solution. I₁ and I₂ of each species were extracted separately
 524 from the combined PE signal via fitting, and $R = I_2/I_1$ was calculated. The result is compared against
 525 $R_{ideal} = x-1, y-1$, calculated from the number of carbons which contribute to I₂. Below each entry we also
 526 present R / R_{ideal} in bold. A value of $R / R_{ideal} > 1$ ($R / R_{ideal} < 1$) indicates a preferable orientation with
 527 the chain (the functional group) closer towards the surface. Values marked with a star (*) in panel (A)
 528 for mixtures of C_x with A₆ are no fit results, since these values were constrained during the fitting to
 529 reach a stable outcome for the strongly overlapping p₂ peaks of C_x/A₆; values were chosen to represent
 530 averages of the results from the other C_x/A_y mixtures with $y < 6$.

(A) C _x	R _{ideal}	no A _y	A1	A2	A4	A6
C2	1	$R = 1.21$	1.39	1.24	1.14	1.25*
		$R/R_{ideal} = 1.21$	1.39	1.24	1.14	1.25*
C4	3	3.63	3.67	3.63	4.27	3.79*
		1.21	1.22	1.21	1.42	1.26*
C6	5	6.80	6.81	6.76	6.78	6.80*
		1.36	1.36	1.35	1.36	1.36*

531

(B) A _y	R _{ideal}	no C _x	C1	C2	C4	C6
A2	1	$R = 0.87$	0.84	0.82	0.88	1.00
		$R/R_{ideal} = 0.87$	0.84	0.82	0.88	1.00
A4	3	2.77	2.76	2.82	2.76	3.69
		0.92	0.92	0.94	0.92	1.23
A6	5	5.09	4.49	4.68	6.14	9.91
		1.02	0.88	0.94	1.23	1.98

532

533 Surface composition

534 We discussed that the surface propensity of the single species increases with the number of carbons
 535 x, y , and that cooperative ion-ion interactions lead to an additional increase of surface propensity for
 536 the mixed solutions. How do these two effects combined influence the relative amounts of C_x and A_y
 537 at the surface? In Table 6, we summarize the ratio $I_{surf, norm}(A_y)/I_{surf, norm}(C_x)$, *i.e.*, the ratio of the total
 538 intensities for each species, which is an indirect measure of the amount of A_y molecules relative to the
 539 amount of C_x molecules at the surface. We observed that the ratio is larger than unity when the C_x
 540 moiety has a short (C2) or no chain (C1), *i.e.*, the surfaces of these solutions are dominated by the A_y
 541 species. For C_x with longer chains, C4 and C6, combined with short-chained A_y, A1 and A2, the
 542 situation is reversed, *i.e.*, the ratio is smaller than unity. If the chains of both molecules are long, then



543 the ratio converges to 1 (a 1:1 molecule ratio), which is expected when considering that a mutual charge
 544 neutralization would favor equal amounts of cationic C_x and anionic A_y species at the surface. Note
 545 that A₆ is a longer molecule than C₆ because of the nitrogen in the functional group, which explains
 546 the larger than unity intensity ratio for C_x/A₆ (with x = 4,6), *i.e.*, the A₆ molecule is likely protruding
 547 out further when both are aligned upright at the surface. We conclude that the species with the longer
 548 chain dominate the surface of the mixed solutions, and if both species contain long carbon chains, they
 549 are present in approximately equal amounts.

550 **Table 6:** Relative surface contribution of A_y versus C_x to the C 1s PE spectra of the mixed solutions,
 551 *i.e.*, an intensity ratio obtained as $I_{\text{surf, norm}}(\text{A}_y)/I_{\text{surf, norm}}(\text{C}_x)$. Errors are calculated via error propagation,
 552 and can get large if the denominator is very small (such as for C1/A2).

	A1	A2	A4	A6
C1	2.12 ± 0.94	21.1 ± 17.4	4.55 ± 0.15	3.35 ± 0.05
C2	1.27 ± 0.13	1.88 ± 0.15	2.77 ± 0.05	2.45 ± 0.05
C4	0.57 ± 0.05	0.84 ± 0.05	1.09 ± 0.05	1.46 ± 0.05
C6	0.68 ± 0.05	0.69 ± 0.05	1.11 ± 0.05	1.60 ± 0.05

553

554 Amount of carbon at the surface

555 So far, we discussed the number density of organic molecular ions at the surface. However, some
 556 atmospherically relevant aspects, such as the availability of carbon for reactions with incoming radicals
 557 and the effects on water accommodation, rather scale with the absolute amount of carbon. (Davies et al.,
 558 2013; Ergin and Takahama, 2016; Miles et al., 2016; Ruehl et al., 2016; Shiraiwa et al., 2011) Here, the
 559 total C 1s surface intensity, $I_{\text{surf}} = I_{\text{tot}} - I_{\text{tot}}(\text{C1})$, *i.e.*, not normalized by the number of carbons (x,y),
 560 provides a measure of how the amount of surface carbon varies. These values are summarized in Table 7.
 561 Since molecular ions with higher surface propensity also tend to contain more carbon atoms, the amount
 562 of carbon at the surface scales even stronger with the alkyl chain length than the amount of organic
 563 molecular ions itself. For example, the relative amount of carbon at the surface is ~1400 times higher
 564 for C₆/A₆ than for C₁/A₁.

565 **Table 7:** Relative amounts of carbon at the surface, expressed as the total intensity minus the bulk
 566 contribution $I_{\text{surf}} = I_{\text{tot}} - I_{\text{tot}}(\text{C1})$.

	A1	A2	A4	A6
single	0.20	2.46	24.5	124
mix:				



C1	0	---	0.19	1.82	16.4	82.8
C2	1.38	---	1.49	3.10	21.6	92.0
C4	10.5	---	8.11	12.9	57.3	179
C6	54.5	---	53.8	80.3	199	268

567

568 **Implications for inorganic ions**

569 Another aspect of the surface enrichment of organic molecular ions concerns their ability to draw
570 inorganic ions to the surface. Inorganic ions such as halides are important in atmospheric chemistry, as
571 exemplified by the ozone depletion through a reaction with iodide and bromide,(Moreno et al., 2018;
572 Chen et al., 2021) the production of Cl_2 from OH (gas) and Cl^- (aq),(Laskin et al., 2006) and the reaction
573 between N_2O_5 (gas) and Br^- (aq).(Sobyra et al., 2019) These reactions involve a gas-phase species and
574 a solvated halide ion, hinging on the presence of the latter at the surface. In single-solute solutions, the
575 inorganic ions act as counterions to the surface-enriched organic ions, which leads to the formation of
576 an electric double layer where organic ions occupy the surface and inorganic ions reside in a sub-layer
577 underneath. The considerable enrichment of either positively or negatively charged organic ions on the
578 surface has been shown to lead to a notable increase in the concentration of inorganic counterions within
579 this sub-layer.(Gopakumar et al., 2022) However, in mixed cationic–anionic molecular ion solutions,
580 the inorganic ions are not the main counter ions of the organic ions, as discussed above. As a result, the
581 inorganic counter ions can be expected to exhibit reduced enrichment in the sub-layer of such mixed
582 cationic–anionic molecular ion solutions (compare Figure 4), and hence fewer ions are available for
583 reactions with gas-phase species.

584

585 **Atmospheric implications**

586 Organic matter is ubiquitous in atmospheric aerosols, both on land and in the ocean, from the tropics to
587 the Arctic. Many organic substances are surface active to a certain extent and also contain
588 (de)protonatable groups such as amino and carboxyl groups, forming molecular ions in a broad pH
589 range from slightly below 5 to somewhat above 10. On the microscopic level, the surface composition
590 of aqueous aerosols has been discussed in terms of solvent-solute interaction, and we show here that
591 solute-solute interactions can also substantially increase the amounts of organics at the surface.

592 The presence of an outer organics-enriched layer has been shown to influence a number of relevant
593 properties and processes, such as optical properties and shortwave radiative effects, water
594 accommodation, and chemical aging, see for example, Refs. (McFiggans et al., 2006; [George et al.,](#)
595 [2010](#); Shiraiwa et al., 2011; Sareen et al., 2013; Davies et al., 2013; Ergin and Takahama, 2016; Miles
596 et al., 2016; Ruehl et al., 2016, Ovadnevaite et al., 2017; Lowe et al., 2019).



597 Organics at the surface lower the surface tension, which is most relevant for the present study. This
598 directly affects aerosol droplet formation, as described by classic Köhler theory (Köhler, H. 1936;
599 [McFiggans et al., 2006](#)), and leads to significant enhancements of cloud condensation nuclei (Sareen et
600 al., 2013; Ovadnevaite et al., 2017). Furthermore, the amphiphilic organics at the surface tend to be
601 oriented with the carbon chains outwards. These organics can form a hydrophobic film, which, on the
602 microscopic scale, will reduce the sticking coefficient of incoming water molecules and thereby affect
603 water accommodation, as well as reducing the frequency of water molecules leaving the liquid phase,
604 i.e., reduce evaporation ([McFiggans et al., 2006](#); Davies et al., 2013; Ergin and Takahama, 2016; Miles
605 et al. 2016; Ruehl et al., 2016). Yet another aspect is that surface species are more accessible than bulk-
606 solvated species for reactions with atmospheric radicals. The cooperatively enhanced surface propensity
607 sets the stage for further chemistry, as surface species are chemically more active than those in the
608 aerosol bulk. This affects e.g. the aerosol chemical aging, *i.e.*, the time evolution of the chemical
609 composition via chemical and photochemical processes ([McFiggans et al., 2006](#); George et al., 2010;
610 Shiraiwa et al., 2011). These three examples illustrate how surface enrichment of organics influences
611 atmospherically fundamental surface properties and processes.

612 On the microscopic scale, many common amphiphilic organics containing amino and carboxyl groups
613 are strongly surface enriched by solute-solvent interactions, implying that modeling aqueous aerosols
614 as homogenous droplets would be inadequate for surface-related phenomena. Our present results show
615 that the surface propensity can be further strongly enhanced in a wide and environmentally relevant pH
616 range by solute-solute interactions, mainly between the oppositely charged molecular ions. This implies
617 that to properly model the surface composition of aqueous aerosols, and hence all surface related
618 properties and processes, such cooperative effects boosting the single-solute surface propensity would
619 have to be considered.

620 On the macroscopic scale, these changes in surface composition can, therefore, significantly influence
621 radiative forcing *via* aerosol growth, cloud condensation nuclei activity, and aerosol chemical aging.
622 Our results demonstrate the principle feasibility of a more advanced input for creating parameterized
623 descriptions of aerosol surface composition needed to properly account for their impacts in climate
624 models. Specifically, the observed drastic increase in surfactant density due to the molecular
625 interactions between different types of organic surfactants would be one effect to be included in future
626 modeling, e.g., cloud droplet formation.

627 **Conclusions**

628 The ionic alkyl amines and carboxylic acids, crucial in the atmosphere as organic compounds, are
629 prevalent over their non-ionic forms in solutions at pHs near 7. We investigated the composition of
630 surfaces in aqueous solutions containing single-component as well as mixtures of the carboxylic acid



631 cations formate, acetate, butyrate, hexanoate and the alkyl amine anions methylammonium,
632 ethylammonium, butylammonium, hexylammonium, relevant in an atmospheric context. By using
633 surface-sensitive X-ray-based PES measurements, we show that mixtures of these compounds exhibit
634 a notable surface enrichment in organic ions compared to solutions with just one species. The
635 availability of molecular ions at the surface scales exponentially as a function of carbon chain length,
636 yielding an increase of up to a factor ~ 230 of the molecular number density, and ~ 1400 times the amount
637 of carbon between mixtures of the smallest species and the largest species studied here. This enrichment
638 arises mainly from ion-pairing interactions of the two ionic species, even at low bulk concentrations.
639 Yet, surface saturation imposes a limit on the maximum achievable enrichment. From this result, it is
640 anticipated that even small variations in composition with admixture of different species can lead to
641 significant changes of atmospherically relevant surface properties and processes such as surface tension,
642 condensation rates, evaporation rates, water accommodation, and the chemical aging of aerosols.
643 Furthermore, changes in the surface composition and condition may significantly impact radiative
644 forcing at a larger scale *via* aerosol growth and cloud condensation nuclei activity. Our findings
645 underscore the necessity for a comprehensive understanding of the surface composition of aqueous
646 solutions of organic molecules, which is a critical aspect for enhancing the accuracy of aerosol modeling
647 within climate models.

648 **Author Contributions**

649 G. Ö. and O. B. conceived the experiments. H. K., S. G., B. C., F. T., D. V., R. M., J. P., H. B., A. N.
650 B., G. Ö., B. W., and O. B. planned, prepared, carried out the experiments, and discussed the data. H.
651 K. and S. T. analyzed the data. S. T., B. W., and O. B. wrote the manuscript with feedback from all
652 authors.

653 **Data Availability**

654 The data of relevance to this study have been deposited at the following DOI:
655 10.5281/zenodo.12644491.

656 **Conflicts of interest**

657 There are no conflicts to declare.



658 Acknowledgements

659 We acknowledge DESY (Hamburg, Germany), a member of the Helmholtz Association HGF, for the
660 provision of experimental facilities. Parts of this research were carried out at PETRA III, and we would
661 like to thank Moritz Hoesch and his team for assistance in using beamline P04. Beamtime was allocated
662 for proposal I-20220937 EC. H.K. and B.W. acknowledge funding from the European Research Council
663 (ERC) under the European Union's Horizon 2020 research and innovation programme (grant agreement
664 No. 883759, AQUACHIRAL). S.T. acknowledges support from the JSPS KAKENHI Grant No.
665 JP20K15229 and ISHIZUE 2024 of Kyoto University. F.T. acknowledges funding by the Deutsche
666 Forschungsgemeinschaft (DFG, German Research Foundation) - Project 509471550, Emmy Noether
667 Programme. F.T. and B.W. acknowledge support by the MaxWater initiative of the Max-Planck-
668 Gesellschaft. O.B. acknowledges support from the Swedish Research Council (VR) through Project
669 2023-04346 and the Swedish Foundation for International Cooperation in Research and Higher
670 Education (STINT) through Project 202100-2932. R.M., J.P., and A.N.B. acknowledge support from
671 the Swedish-Brazilian collaboration STINT-CAPES process no. 88881.465527/2019-01. ANB
672 acknowledges support from FAPESP (the Sao Paulo Research Foundation, Process number
673 2017/11986-5) and Shell and ANP (Brazil's National Oil, Natural Gas and Biofuels Agency); and
674 CNPq-Brazil process 401581/2016-0.

675 References

676 Bagschik, K., Wagner, J., Buß, R., Riepp, M., Philippi-Kobs, A., Müller, L., Buck, J., Trinter, F.,
677 Scholz, F., Seltmann, J., Hoesch, M., Viefhaus, J., Grübel, G., Oepen, H. P., and Frömter, R.: Direct
678 2D spatial-coherence determination using the Fourier-analysis method: multi-parameter
679 characterization of the P04 beamline at PETRA III, *Optics Express*, 28, 10.1364/oe.382608, 2020.
680 Björneholm, O., Öhrwall, G., de Brito, A. N., Ågren, H., and Carravetta, V.: Superficial Tale of Two
681 Functional Groups: On the Surface Propensity of Aqueous Carboxylic Acids, Alkyl Amines, and
682 Amino Acids, *Acc. Chem. Res.*, 55, 3285-3293, 10.1021/acs.accounts.2c00494, 2022.
683 Chen, S., Artiglia, L., Orlando, F., Edebeli, J., Kong, X., Yang, H., Boucly, A., Corral Arroyo, P.,
684 Prisle, N., and Ammann, M.: Impact of Tetrabutylammonium on the Oxidation of Bromide by Ozone,
685 *ACS Earth and Space Chemistry*, 5, 3008-3021, 10.1021/acsearthspacechem.1c00233, 2021.
686 Davies, J. F., Miles, R. E. H., Haddrell, A. E., and Reid, J. P.: Influence of organic films on the
687 evaporation and condensation of water in aerosol, *Proceedings of the National Academy of Sciences*,
688 110, 8807-8812, 10.1073/pnas.1305277110, 2013.
689 Dupuy, R., Filser, J., Richter, C., Buttersack, T., Trinter, F., Gholami, S., Seidel, R., Nicolas, C.,
690 Bozek, J., Egger, D., Oberhofer, H., Thürmer, S., Hergenhan, U., Reuter, K., Winter, B., and Bluhm,



- 691 H.: Ångström-Depth Resolution with Chemical Specificity at the Liquid-Vapor Interface, *Phys. Rev.*
692 *Lett.*, 130, 10.1103/PhysRevLett.130.156901, 2023.
- 693 Ekholm, V.: Ion pairing and Langmuir-like adsorption at aqueous surfaces studied by core-level
694 spectroscopy, Doctoral thesis, comprehensive summary, Digital Comprehensive Summaries of
695 Uppsala Dissertations from the Faculty of Science and Technology, Acta Universitatis Upsaliensis,
696 Uppsala, 62 pp., <http://uu.diva-portal.org/smash/get/diva2:1244545/PREVIEW01.jpg>, 2018.
- 697 Ekholm, V., Coleman, C., Björnhal Prytz, N., Walz, M.-M., Werner, J., Öhrwall, G., Rubensson, J.-
698 E., and Björneholm, O.: Strong enrichment of atmospherically relevant organic ions at the aqueous
699 interface: the role of ion pairing and cooperative effects, *Phys. Chem. Chem. Phys.*, 20, 27185-27191,
700 10.1039/c8cp04525a, 2018.
- 701 Ergin, G. and Takahama, S.: Carbon Density Is an Indicator of Mass Accommodation Coefficient of
702 Water on Organic-Coated Water Surface, *J. Phys. Chem. A*, 120, 2885-2893,
703 10.1021/acs.jpca.6b01748, 2016.
- 704 George, I., Abbatt, J. Heterogeneous oxidation of atmospheric aerosol particles by gas-phase
705 radicals. *Nature Chem* 2, 713–722, 10.1038/nchem.806, 2010.
- 706 Goldstein, A. H. and Galbally, I. E.: Known and Unexplored Organic Constituents in the Earth's
707 Atmosphere, *Environ. Sci. Technol.*, 41, 1514-1521, 10.1021/es072476p, 2007.
- 708 Gopakumar, G., Unger, I., Saak, C.-M., Öhrwall, G., Naves de Brito, A., Rizuti da Rocha, T. C.,
709 Nicolas, C., Coleman, C., and Björneholm, O.: The surface composition of amino acid – halide salt
710 solutions is pH-dependent, *Environmental Science: Atmospheres*, 2, 441-448, 10.1039/d1ea00104c,
711 2022.
- 712 Grushka, E.: Characterization of exponentially modified Gaussian peaks in chromatography, *Anal.*
713 *Chem.*, 44, 1733-1738, 10.1021/ac60319a011, 1972.
- 714 Hüfner, S., Schmidt, S., and Reinert, F.: Photoelectron spectroscopy—An overview, *Nuclear*
715 *Instruments and Methods in Physics Research Section A: Accelerators, Spectrometers, Detectors and*
716 *Associated Equipment*, 547, 8-23, 10.1016/j.nima.2005.05.008, 2005.
- 717 Jimenez, J. L., Canagaratna, M. R., Donahue, N. M., Prevot, A. S. H., Zhang, Q., Kroll, J. H.,
718 DeCarlo, P. F., Allan, J. D., Coe, H., Ng, N. L., Aiken, A. C., Docherty, K. S., Ulbrich, I. M.,
719 Grieshop, A. P., Robinson, A. L., Duplissy, J., Smith, J. D., Wilson, K. R., Lanz, V. A., Hueglin, C.,
720 Sun, Y. L., Tian, J., Laaksonen, A., Raatikainen, T., Rautiainen, J., Vaattovaara, P., Ehn, M.,
721 Kulmala, M., Tomlinson, J. M., Collins, D. R., Cubison, M. J., Dunlea, J., Huffman, J. A., Onasch, T.
722 B., Alfarra, M. R., Williams, P. I., Bower, K., Kondo, Y., Schneider, J., Drewnick, F., Borrmann, S.,
723 Weimer, S., Demerjian, K., Salcedo, D., Cottrell, L., Griffin, R., Takami, A., Miyoshi, T.,
724 Hatakeyama, S., Shimojo, A., Sun, J. Y., Zhang, Y. M., Dzepina, K., Kimmel, J. R., Sueper, D.,
725 Jayne, J. T., Herndon, S. C., Trimborn, A. M., Williams, L. R., Wood, E. C., Middlebrook, A. M.,
726 Kolb, C. E., Baltensperger, U., and Worsnop, D. R.: Evolution of Organic Aerosols in the
727 Atmosphere, *Science*, 326, 1525-1529, 10.1126/science.1180353, 2009.



- 728 Kanakidou, M., Seinfeld, J. H., Pandis, S. N., Barnes, I., Dentener, F. J., Facchini, M. C., Van
729 Dingenen, R., Ervens, B., Nenes, A., Nielsen, C. J., Swietlicki, E., Putaud, J. P., Balkanski, Y., Fuzzi,
730 S., Horth, J., Moortgat, G. K., Winterhalter, R., Myhre, C. E. L., Tsigaridis, K., Vignati, E.,
731 Stephanou, E. G., and Wilson, J.: Organic aerosol and global climate modelling: a review, *Atmos.*
732 *Chem. Phys.*, 5, 1053-1123, 10.5194/acp-5-1053-2005, 2005.
- 733 Köhler H., The nucleus in and the growth of hygroscopic droplets, *Trans. Faraday Soc.* 32, 1152-1161,
734 10.1039/TF9363201152, 1936
- 735 Laskin, A., Wang, H., Robertson, W. H., Cowin, J. P., Ezell, M. J., and Finlayson-Pitts, B. J.: A New
736 Approach to Determining Gas-Particle Reaction Probabilities and Application to the Heterogeneous
737 Reaction of Deliquesced Sodium Chloride Particles with Gas-Phase Hydroxyl Radicals, *J. Phys.*
738 *Chem. A*, 110, 10619-10627, 10.1021/jp063263+, 2006.
- 739 Lee, M.-T., Orlando, F., Artiglia, L., Chen, S., and Ammann, M.: Chemical Composition and
740 Properties of the Liquid–Vapor Interface of Aqueous C1 to C4 Monofunctional Acid and Alcohol
741 Solutions, *J. Phys. Chem. A*, 120, 9749-9758, 10.1021/acs.jpca.6b09261, 2016.
- 742 Lowe, S. J., Partridge, D. G., Davies, J. F., Wilson, K. R., Topping, D., and Riipinen, I.: Key drivers
743 of cloud response to surface-active organics, *Nat. Commun.*, 10, 10.1038/s41467-019-12982-0, 2019.
- 744 Malerz, S., Haak, H., Trinter, F., Stephansen, A. B., Kolbeck, C., Pohl, M., Hergenahhn, U., Meijer,
745 G., and Winter, B.: A setup for studies of photoelectron circular dichroism from chiral molecules in
746 aqueous solution, *Rev. Sci. Instrum.*, 93, 015101, 10.1063/5.0072346, 2022.
- 747 Malerz, S., Trinter, F., Hergenahhn, U., Ghrist, A., Ali, H., Nicolas, C., Saak, C.-M., Richter, C.,
748 Hartweg, S., Nahon, L., Lee, C., Goy, C., Neumark, D. M., Meijer, G., Wilkinson, I., Winter, B., and
749 Thürmer, S.: Low-energy constraints on photoelectron spectra measured from liquid water and
750 aqueous solutions, *Phys. Chem. Chem. Phys.*, 23, 8246-8260, 10.1039/d1cp00430a, 2021.
- 751 McFiggans, G., Artaxo, P., Baltensperger, U., Coe, H., Facchini, M. C., Feingold, G., Fuzzi, S.,
752 Gysel, M., Laaksonen, A., Lohmann, U., Mentel, T. F., Murphy, D. M., O'Dowd, C. D., Snider, J. R.,
753 and Weingartner, E.: The effect of physical and chemical aerosol properties on warm cloud droplet
754 activation, *Atmos. Chem. Phys.*, 6, 2593–2649, <https://doi.org/10.5194/acp-6-2593-2006>, 2006.
- 755 McCormick, R. A. and Ludwig, J. H.: Climate Modification by Atmospheric Aerosols, *Science*, 156,
756 1358-1359, 10.1126/science.156.3780.1358, 1967.
- 757 Miles, R. E. H., Davies, J. F., and Reid, J. P.: The influence of the surface composition of mixed
758 monolayer films on the evaporation coefficient of water, *Phys. Chem. Chem. Phys.*, 18, 19847-19858,
759 10.1039/c6cp03826c, 2016.
- 760 Minofar, B., Jungwirth, P., Das, M. R., Kunz, W., and Mahiuddin, S.: Propensity of Formate, Acetate,
761 Benzoate, and Phenolate for the Aqueous Solution/Vapor Interface: Surface Tension Measurements
762 and Molecular Dynamics Simulations, *J. Phys. Chem. C*, 111, 8242-8247, 10.1021/jp068804+, 2007.



- 763 Mocellin, A., Gomes, A. H. d. A., Araújo, O. C., de Brito, A. N., and Björneholm, O.: Surface
764 Propensity of Atmospherically Relevant Amino Acids Studied by XPS, *J. Phys. Chem. B*, 121, 4220-
765 4225, 10.1021/acs.jpcc.7b02174, 2017.
- 766 Moreno, C. G., Gálvez, O., López-Arza Moreno, V., Espildora-García, E. M., and Baeza-Romero, M.
767 T.: A revisit of the interaction of gaseous ozone with aqueous iodide. Estimating the contributions of
768 the surface and bulk reactions, *Phys. Chem. Chem. Phys.*, 20, 27571-27584, 10.1039/c8cp04394a,
769 2018.
- 770 Noziere, B.: Don't forget the surface, *Science*, 351, 1396-1397, 10.1126/science.aaf3253, 2016.
- 771 Öhrwall, G., Prisle, N. L., Ottosson, N., Werner, J., Ekholm, V., Walz, M.-M., and Björneholm, O.:
772 Acid–Base Speciation of Carboxylate Ions in the Surface Region of Aqueous Solutions in the
773 Presence of Ammonium and Aminium Ions, *J. Phys. Chem. B*, 119, 4033-4040, 10.1021/jp509945g,
774 2015.
- 775 Ottosson, N., Wernersson, E., Söderstrom, J., Pokapanich, W., Kaufmann, S., Svensson, S., Persson,
776 I., Öhrwall, G., and Björneholm, O.: The Protonation State of Small Carboxylic Acids at the Water
777 Surface from Photoelectron Spectroscopy, *Phys. Chem. Chem. Phys.*, 13, 12261-12267,
778 10.1039/c1cp20245f, 2011.
- 779 Ovadnevaite, J., Zuend, A., Laaksonen, A., Sanchez, K. J., Roberts, G., Ceburnis, D., Decesari, S.,
780 Rinaldi, M., Hodas, N., Facchini, M. C., Seinfeld, J. H., and O' Dowd, C.: Surface tension prevails
781 over solute effect in organic-influenced cloud droplet activation, *Nature*, 546, 637-641,
782 10.1038/nature22806, 2017.
- 783 Powis, I., Holland, D. M. P., Antonsson, E., Patanen, M., Nicolas, C., Miron, C., Schneider, M.,
784 Soshnikov, D. Y., Dreuw, A., and Trofimov, A. B.: The influence of the bromine atom Cooper
785 minimum on the photoelectron angular distributions and branching ratios of the four outermost bands
786 of bromobenzene, *J. Chem. Phys.*, 143, 144304, 10.1063/1.4931642, 2015.
- 787 Ruehl, C. R., Davies, J. F., and Wilson, K. R.: An interfacial mechanism for cloud droplet formation
788 on organic aerosols, *Science*, 351, 1447-1450, 10.1126/science.aad4889, 2016.
- 789 Sareen, N., Schwier, A. N., Lathem, T. L., Nenes, A., and McNeill, V. F.: Surfactants from the gas
790 phase may promote cloud droplet formation, *Proceedings of the National Academy of Sciences*, 110,
791 2723-2728, 10.1073/pnas.1204838110, 2013.
- 792 Sasaki, S.: Analyses for a planar variably-polarizing undulator, *Nuclear Instruments and Methods in*
793 *Physics Research Section A: Accelerators, Spectrometers, Detectors and Associated Equipment*, 347,
794 83-86, 10.1016/0168-9002(94)91859-7, 1994.
- 795 Shiraiwa, M., Ammann, M., Koop, T., and Pöschl, U.: Gas uptake and chemical aging of semisolid
796 organic aerosol particles, *Proceedings of the National Academy of Sciences*, 108, 11003-11008,
797 10.1073/pnas.1103045108, 2011.



- 798 Sobyra, T. B., Pliszka, H., Bertram, T. H., and Nathanson, G. M.: Production of Br₂ from N₂O₅ and
799 Br⁻ in Salty and Surfactant-Coated Water Microjets, *The Journal of Physical Chemistry A*, 123, 8942-
800 8953, 10.1021/acs.jpca.9b04225, 2019.
- 801 Thürmer, S., Seidel, R., Faubel, M., Eberhardt, W., Hemminger, J. C., Bradforth, S. E., and Winter,
802 B.: Photoelectron Angular Distributions from Liquid Water: Effects of Electron Scattering, *Phys. Rev.*
803 *Lett.*, 111, 173005, 10.1103/PhysRevLett.111.173005, 2013.
- 804 The Intergovernmental Panel on Climate Change (IPCC): *Climate Change 2022: Impacts, Adaptation*
805 *and Vulnerability*, 2022.
- 806 Tsigaridis, K., Daskalakis, N., Kanakidou, M., Adams, P. J., Artaxo, P., Bahadur, R., Balkanski, Y.,
807 Bauer, S. E., Bellouin, N., Benedetti, A., Bergman, T., Berntsen, T. K., Beukes, J. P., Bian, H.,
808 Carslaw, K. S., Chin, M., Curci, G., Diehl, T., Easter, R. C., Ghan, S. J., Gong, S. L., Hodzic, A.,
809 Hoyle, C. R., Iversen, T., Jathar, S., Jimenez, J. L., Kaiser, J. W., Kirkevåg, A., Koch, D., Kokkola,
810 H., Lee, Y. H., Lin, G., Liu, X., Luo, G., Ma, X., Mann, G. W., Mihalopoulos, N., Morcrette, J. J.,
811 Müller, J. F., Myhre, G., Myriokefalitakis, S., Ng, N. L., O'Donnell, D., Penner, J. E., Pozzoli, L.,
812 Pringle, K. J., Russell, L. M., Schulz, M., Sciare, J., Seland, Ø., Shindell, D. T., Sillman, S., Skeie, R.
813 B., Spracklen, D., Stavroukou, T., Steenrod, S. D., Takemura, T., Tiitta, P., Tilmes, S., Tost, H., van
814 Noije, T., van Zyl, P. G., von Salzen, K., Yu, F., Wang, Z., Wang, Z., Zaveri, R. A., Zhang, H.,
815 Zhang, K., Zhang, Q., and Zhang, X.: The AeroCom evaluation and intercomparison of organic
816 aerosol in global models, *Atmos. Chem. Phys.*, 14, 10845-10895, 10.5194/acp-14-10845-2014, 2014.
- 817 Twomey, S.: Pollution and the planetary albedo, *Atmospheric Environment* (1967), 8, 1251-1256,
818 10.1016/0004-6981(74)90004-3, 1974.
- 819 Viehhaus, J., Scholz, F., Deinert, S., Glaser, L., Ilchen, M., Seltmann, J., Walter, P., and Siewert, F.:
820 The Variable Polarization XUV Beamline P04 at PETRA III: Optics, mechanics and their
821 performance, *Nucl. Instrum. Methods Phys. Res., Sect. A*, 710, 151-154, 10.1016/j.nima.2012.10.110,
822 2013.
- 823 Walz, M. M., Werner, J., Ekholm, V., Prisle, N. L., Öhrwall, G., and Björneholm, O.: Alcohols at the
824 aqueous surface: chain length and isomer effects, *Phys. Chem. Chem. Phys.*, 18, 6648-6656,
825 10.1039/c5cp06463e, 2016.
- 826 Walz, M. M., Coleman, C., Werner, J., Ekholm, V., Lundberg, D., Prisle, N. L., Öhrwall, G., and
827 Björneholm, O.: Surface behavior of amphiphiles in aqueous solution: a comparison between different
828 pentanol isomers, *Phys. Chem. Chem. Phys.*, 17, 14036-14044, 10.1039/c5cp01870f, 2015.
- 829 Werner, J., Persson, I., Björneholm, O., Kawecki, D., Saak, C.-M., Walz, M.-M., Ekholm, V., Unger,
830 I., Valtl, C., Coleman, C., Öhrwall, G., and Prisle, N. L.: Shifted equilibria of organic acids and bases
831 in the aqueous surface region, *Phys. Chem. Chem. Phys.*, 20, 23281-23293, 10.1039/c8cp01898g,
832 2018.
- 833 Winter, B. and Faubel, M.: Photoemission from Liquid Aqueous Solutions, *Chem. Rev.*, 106, 1176-
834 1211, Doi 10.1021/Cr040381p, 2006.